A New Catalog of Silicate Carbon Stars

Young-Joo Kwon and Kyung-Won Suh

Department of Astronomy and Space Science, Chungbuk National University, Cheongju 361-763, Korea
kwsuh@chungbuk.ac.kr

Abstract: A silicate carbon star is a carbon star which shows circumstellar silicate dust features. We collect a sample of 44 silicate carbon stars from the literature and investigate the validity of the classification. For some objects, it is uncertain whether the central star is a carbon star. We confirm that 29 objects are verified silicate carbon stars. We classify the confirmed objects into three subclasses based on the evolution phase of the central star. To investigate the effect of the chemical transition phase from O to C, we use the radiative transfer models for the detached silicate dust shells. The spectral energy distributions and the infrared two-color diagrams of the silicate carbon stars are compared with the theoretical model results. For the chemical transition model without considering the effect of a disk, we find that the life time of the silicate feature is about 50 to 400 years depending on the initial dust optical depth.

Key words: stars: AGB stars — infrared: stars — circumstellar matter — masers — dust: extinction

1. Introduction

A silicate carbon star (hereafter; SCS) is a carbon star which shows circumstellar silicate dust features. They were discovered by the IRAS observations (Little-Marenin 1986; Willems & de Jong 1986). So far, about 35 SCSs have been identified in our Galaxy (e.g., Suh & Kwon 2011).

As stars evolve into the thermal pulsing asymptotic giant branch (AGB) phase, the abundances of some elements in the stellar atmosphere may change by the episodic third dredge-up process after each thermal pulse. The stepwise increase of the carbon abundance is related to the formation of a carbon star because the C/O abundance ratio can change from C/O < 1 to C/O > 1 (e.g., Busso et al. 1999). These stars may experience the S star phase before they become carbon stars when the C/O ratio is close to 1. When AGB stars of intermediate mass range go through carbon dredge-up processes, the abundance of carbon becomes larger than that of oxygen, O-rich dust grain formation ceases, and the stars become visual carbon stars. After that phase, C-rich dust grains start forming (Iben 1981; Chan & Kwok 1990; Groenewegen et al. 1995; Suh 2000).

Willems & de Jong (1986) and Chan & Kwok (1991) suggested that SCSs are in transition from O-rich AGB stars to carbon stars. Many of the SCSs are fairly well fitted with a simple detached silicate dust shell model. However, this scenario could be unlikely because the time scale for such a transitional object to be observed as a SCS is predicted to be too short.

A more promising scenario suggests that SCSs have a low-luminosity companion, possibly a dwarf star (e.g., Morris 1987; Lloyd Evans 1990; Yamamura et al. 2000). A relatively long-lived disk of silicate dust is supposed to be formed when the primary was still an O-rich AGB star. When the primary star was an M-type giant and O-rich materials were supposed to be used to form a circumbinary (or circum-companion) disk. The disk may serve as a reservoir of O-rich material even after the star undergoes thermal pulses and evolves into a carbon star.

For a large sample of AGB stars, infrared observational data are available from the Infrared Astronomical Satellite (IRAS), Infrared Space Observatory (ISO), Midcourse Space Experiment (MSX), USNO-B1.0 (Monet et al. 2003), Two-Micron All-Sky Survey (2MASS), Wide-field Infrared Survey Explorer (WISE) and AKARI. The IRAS point source catalog (PSC) version 2.1 contains useful photometric data in four bands (12, 25, 50 and 100 μm). The MSX (Egan et al. 2003) PSC provides useful photometric data in 8.28, 12.13, 14.65, 21.34 μm wavelength bands. The 2MASS (Cutri et al. 2003) PSC contains accurate positions and fluxes for about 470 million stars and other unresolved objects in J (1.25 μm), H (1.65 μm) and K (2.17 μm) bands. The WISE (Wright et al. 2010) surveyed the entire sky with much higher sensitivity than previous missions. The AKARI space telescope (Murakami et al. 2007) made an all sky survey with the infrared camera (IRC) and far infrared surveyor (FIS). We may use the AKARI PSC data in two bands (9 and 18 μm) obtained by the IRC and the bright-source catalogue (BSC) data in four bands (65, 90, 140 and 160 μm) obtained by the FIS.

The IRAS Low Resolution Spectrograph (LRS; $\lambda = 8-22$ μm) data are useful to identify important dust features of SCSs. Kwok et al. (1997) used IRAS LRS to identify the class E (the 10 μm silicate feature in emission) and class A (the 10 μm silicate feature in absorption) objects. The ISO Short Wavelength Spectrometer (SWS; $\lambda = 2.4-45.4$ μm) and Spitzer Infrared Spectrograph (IRS; $\lambda = 5.2-38$ μm) provided high res-

olution spectra for some SCSs.

In this paper, we present a new catalog of SCSs. We confirm the C-rich nature of central stars and O-rich nature of circumstellar envelopes for the sample SCSs. To investigate the effect of the chemical transition phase from O to C, we use radiative transfer models for the detached silicate dust shells. We compare the spectral energy distributions and infrared two color diagrams of the SCSs with the theoretical model results and estimate the evolutionary time scales for SCSs.

2. Sample Collection and Confirmation

Suh & Kwon (2011, hereafter SK11) listed 35 SCSs. We have used the 35 objects in SK11 to construct the initial sample of stars to be verified in this paper.

Chen & Shan (2011, hereafter CS11) presented 5 new SCSs which were verified from 17 new candidate objects as well as 34 previously known SCSs. The 12 candidate objects which were not verified to be SCSs by CS11 are regarded as unconfirmed objects (see Section 3). The two objects (IRAS 06176−1036 and 13198−6224) listed in CS11 as previously known SCSs were not listed in SK11. We add those 7 objects to the sample stars (the 5 new SCSs and 2 previously known objects presented in CS11).

We add two more objects: IRAS 19163+2745 (EP Lyr) and IRAS 20451+4552 (CY Cyg). EP Lyr is a post-AGB star which shows both polycyclic aromatic hydrocarbon (PAH) and crystalline silicate features like the Red Rectangle (Gielen et al. 2008, 2009). CY Cyg is a SC type star with silicate emission feature. According to Kwok et al. (1997), there are 4 SC type stars (W Cas, VX Aql, S Lyr and CY Cyg) and a CS type star (IRAS 09083−5158) which are in LRS class E.

Finally, the 44 objects are selected for the sample of SCSs to be verified in this paper and they are listed in Table 1. Because the AKARI PSC measures the flux of the peak emission with a much smaller aperture (9 arcsec beam size) than IRAS PSC, we use the AKARI PSC position for further identification. For the 44 objects, we cross-identify the AKARI PSC counterpart by finding the nearest source within $30''$ using the position information of the IRAS PSC (version 2.1). For each sample star, we have found an AKARI source within $30''$ except for IRAS 16070−4359 which has two AKARI sources. For the IRAS 16070−4359, the counterpart is selected by comparing the flux data with the IRAS PSC.

We use the counterpart of the General Catalog of Galactic Carbon stars (Alksnis et al. 2001, hereafter CGCS) based on the position information of the AKARI PSC as well as the available spectral evidences in optical, infrared and radio regions.

In Table 1, we present the IRAS PSC number, AKARI PSC counterpart, position information from the AKARI PSC counterpart, CGCS counterpart, and IRAS LRS class. For the 44 sample objects, we investigate the validity of the classification. To confirm the nature of the SCS, we investigate the signatures of

the C-rich nature of central star and O-rich nature of circumstellar envelope.

2.1. The CGCS Counterparts

We identify the CGCS counterparts for which the position difference between the AKARI PSC and CGCS is less than $2'$. For the 44 sample stars, we find that 35 objects have the CGCS counterparts and they are listed in Table 1. The position differences (Δr) between the AKARI PSC and CGCS are also listed in Table 1.

For the 35 CGCS counterparts, only 3 sources have position differences larger than $30''$ (IRAS 12364−6539, 16070−4359 and 18252−1011). For the three sources, the AKARI, MSX and 2MASS counterparts based on the IRAS PSC and CGCS positions are different. These objects seem to be different sources. We mark those objects with the asterisk symbol in Table 1. We list the 3 objects as unconfirmed objects in Table 2. These 3 stars with large position differences need more reliable observation data to confirm their nature.

The O-rich nature of the outer shells can be easily recognized by IRAS LRS class by Kwok et al. (1997). Among the 35 stars, 33 stars with silicate emission features are classified as E class, and 2 stars (IRAS 07204−1032 and 12364−6539) as F class. For IRAS 07204−1032, Engels (1994) detected H_2O maser. H_2O maser occurs only in the dusty O-rich environments. The spectral type of the last one, IRAS 12364−6539, is M9 according to Skiff (2014). Note that this is one of the unconfirmed objects with the large position difference between the AKARI and CGCS.

2.2. The Sample Stars without CGCS Couterparts

As mentioned in Section 2.1, 9 stars do not have CGCS counterparts within $3'$. We check these stars using the available optical and infrared spectral information from the literature.

C_2H_2+HCN absorption features around 3.0 μm observed by the ISO SWS are clear evidences of the central carbon star. There are obvious C_2H_2+HCN absorption features for three stars: IRAS 03201+5459, 09425−6040 and 19111+2555 (e.g., Molster et al. 2001). These three stars show amorphous or crystalline silicate features.

IRAS 06176−1036 and 19163+2745 (Red Rectangle and EP Lyr) show the PAH and crystalline silicate features detected by ISO-SWS or Spitzer-IRS (e.g., Gielen et al. 2008, 2009).

Drew et al. (2005) observed the optical spectrum toward IRAS 22146+6111 and identified this star as a carbon star. IRAS 20451+4552 (CY Cyg) is classified as an SC star by Keenan & Boeshaar (1980). Kwok et al. (1997) classified IRAS 21135+5200 as a carbon star. All the 3 stars show a silicate emission feature at 10 μm detected from the IRAS LRS.

However, the remaining one object, IRAS 21444+5053 has no direct evidence of a carbon star. We list it as an unconfirmed object in Table 2. We present a detailed discussion for all of the unconfirmed objects in Section 3.

Table 1
Sample objects for SCSs (44 objects)

IRAS PSC	Other Name	AKARI PSC	R.A. (2000)	Dec. (2000)	CGCS	Δr(arcsec)	LRS	Ref.
00519+5817	W Cas	0054539+583349	13.72478	58.56379	136	0.72	E	SK11; CS11
01373+4000	FBS 0137+400	0140206+401518	25.08616	40.25515	6019	10.44	E	SK11; CS11
03201+5459	-	0323593+551014	50.99747	55.17075	-	-	U	SK11; CS11
06017+1011	NSV 2814	0604313+101056	91.13083	10.18243	1158	28.74	E	SK11; CS11
06176−1036	Red rectangle	0619582−103814	94.99252	-10.63743	-	-	P	CS11
06194+1635	-	0622213+163423	95.58881	16.57326	6139	3.36	E	SK11; CS11
07179+2505	BM Gem	0720590+245958	110.24605	24.99947	1653	0.72	E	SK11; CS11
07204−1032	-	0722469−103839	110.69561	-10.64440	1682	2.94	F	SK11
08002−3803	Hen 38	0802050−381151	120.52102	-38.19763	2011	3	E	SK11; CS11
08577−6035	Mc97 2-11	0858542−604735	134.72621	-60.79326	2406	17.58	E	SK11; CS11
09083−5158	-	0909592−521020	137.49690	-52.17228	2445	39.54	E	SK11; CS11
09411−5933	-	0942361−594737	145.65059	-59.79373	6337	1.98	E	SK11; CS11
09425−6040	-	0944017−605425	146.00731	-60.90697	-	-	U	SK11; CS11
10171−6205	-	1018503−622101	154.70996	-62.35050	6359	0.66	E	SK11; CS11
11048−6046	-	1106546−610301	166.72757	-61.05033	2957	24.84	E	SK11; CS11
11311−6355	-	1133246−641158	173.35264	-64.19952	6450	2.34	E	SK11; CS11
12364−6539	-	1239236−655603	189.84839	-65.93439	3263*	50.52	F	SK11
12569−6105	-	1300043−612118	195.01814	-61.35526	6503	2.52	E	SK11; CS11
13198−6224	RAFGL 4890S	1323088−623954	200.78697	-62.66526	6526	14.16	E	CS11
14286−4706	-	1431574−471943	217.98948	-47.32878	6559	1.32	E	SK11; CS11
15575−5238	-	1601205−524649	240.33542	-52.78041	6610	10.02	E	CS11
16001−4851	-	1603478−485915	240.94942	-48.98765	6612	1.68	E	SK11; CS11
16070−4359	-	1610358−440654	242.64945	-44.11517	3668*	101.1	E	CS11
16103−4929	-	1614054−493658	243.52267	-49.61615	6624	1.62	E	SK11; CS11
16328−4656	-	1636291−470258	249.12155	-47.04954	6650	5.1	E	SK11; CS11
17291−3401	-	1732281−340313	263.11734	-34.05384	3841	4.32	E	SK11
18006−3213	FJF 270	1803527−321259	270.96992	-32.21660	3935	15.3	E	SK11; CS11
18252−1011	-	1828010−100917	277.00444	-10.15479	4015*	106.98	E	SK11; CS11
18575−0139	VX Aql	1900096−013458	285.04029	-1.58291	4152	2.94	E	SK11; CS11
19111+2555	S Lyr	1913117+260027	288.29915	26.00775	-	-	E	SK11; CS11
19139+5412	NC 83	1915015+541729	288.75646	54.29144	4222	3.84	E	SK11; CS11
19163+2745	EP Lyr	1918195+275103	289.58154	27.85093	-	-	-	New
19451+2856	NSV 12406	1947131+290406	296.80466	29.06848	4476	1.56	E	SK11; CS11
19583−0730	V1468 Aql	2001051−072152	300.27158	-7.36445	4595	0.3	E	SK11; CS11
20092+3557	V429 Cyg	2011061+360648	302.77579	36.11347	4729	1.86	E	SK11; CS11
20350+5954	V778 Cyg	2036073+600525	309.03083	60.09049	4923	5.28	E	SK11; CS11
20451+4552	CY Cyg	2046503+460306	311.70962	46.05176	-	-	E	New
20476+4422	-	2049250+443348	312.35417	44.56353	4993	2.94	E	SK11; CS11
21135+5200	-	2115081+521249	318.78392	52.21375	-	-	E	SK11; CS11
21444+5053	-	2146149+510729	326.56247	51.12478	-	-	E	CS11
21566+5309	MQ Cyg	2158261+532412	329.60903	53.40343	5526	1.74	E	SK11; CS11
22146+6111	-	2216197+612621	334.08234	61.43923	-	-	E	CS11
23138+6204	NSV 14477	2316023+622118	349.00976	62.35502	6912	1.98	E	CS11
23176+4658	EU And	2319589+471434	349.99544	47.24282	5848	4.38	E	SK11; CS11

SK11 = Suh & Kwon (2011); CS11 = Chen & Shan (2011). *The object seems to be a different source (See Section 3).

2.3. Two-Color Diagrams

For some sample stars having the CGCS number, they are classified to be carbon stars by the method based on the color index. This method classifies the stars based on their location in a two-color diagram (2CD). Epchtein et al. (1987, 1990) showed that the 2CD using [12]-[25] versus K-L allows to distinguish carbon stars from O-rich stars with some reliability. In the 2CD using [12]-[25] versus K-L, carbon stars are located in the lower region and O-rich stars appear in the upper region. However, it is well known that the position of an AGB star on a 2CD varies widely depending on the phase of pulsation (e.g., Suh 2004). The variation of the positions on 2CDs could lead to mis-classifications especially for the stars near the border.

Therefore, the color index method is not sufficient to reveal the C-rich nature of the central star. For the 10 objects, for which the C-rich nature is solely determined from the 2CD method, we need further verifications. We list these as unconfirmed objects in Table 2.

3. Unconfirmed Objects

Through the investigations described in Section 2, we confirm that 29 objects are real SCSs. But for 15 objects, it is not clear whether the central star is a real carbon star. We list the 15 unconfirmed objects in Table 2.

CS11 presented 12 candidate objects (5 candidates in table 2; 7 probable candidates in Table 3) which were not verified to be real SCSs. In Table 3, we list the 12 candidate objects presented by CS11 which can also be regarded as unconfirmed objects.

For all of the 15 unconfirmed objects, the silicate emission feature at 10 μm is detected in the IRAS LRS spectrum. Kwok et al. (1997) classified them as the IRAS LRS class E.

IRAS 06194+1635 (CGCS 6139): Guglelmo et al. (1993) identified it as a carbon star based on the 2CD using [12]-[25] versus K-L. Althogh the object is in the region of carbon stars, its C-rich nature is not clear (see Section 2.3).

IRAS 09411-5933 (CGCS 6337): This star was identified to be a carbon star by Fouque et al. (1992) using the [12]-[25] and K-L color indices. However, Skiff (2014) identified its spectral type as M2/3. OH maser emission at 1612 MHz was not detected in OH maser survey of te Lintel Hekkert (1991).

IRAS 11311-6355 (CGCS 6450): Guglielmo et al. (1993) first identified it as a carbon star from the 2CD using [12]-[25] versus K-L. Kwok et al. (1997) classified this star as LRS class E with self-absorption. As mentioned above, the color index method is not enough for revealing the C-rich nature of the central star.

IRAS 12364-6539: This star has a large position difference from CGCS 3264 (Δr = 51″). Skiff (2014) identified the spectral type as M9. The AKARI, MSX and 2MASS counterparts based on the IRAS PSC position and CGCS position are different. IRAS 12364-6539 seems to be an O-rich star rather than an SCS.

IRAS 12569-6105 (CGCS 6503): Epchtein et al. (1990) classified it as a carbon star using a 2CD. MacConnell (2000) and Skiff (2014) classified this star as an S star.

IRAS 13198-6224 (CGCS 6610): Aaronson et al. (1989) classified it as a carbon star, but Lloyd Evans (1991) argued that the spectral type is M2.

IRAS 14286-4706 (CGCS 6559): Fouque et al. (1992) firstly identified this object as a carbon star using the [12]-[25] versus K-L 2CD. It is seen near the border region between O-rich AGB stars and carbon stars on the 2CD.

IRAS 16001-4851 (CGCS 6612): Epchtein et al. (1990) identified it as a carbon star using the color index method. Its C-rich nature is not clear

IRAS 16070-4359: Guglielmo et al. (1993) identified it as a carbon star from the 2CD using [12]-[25] versus K-L. However, this star has a large position difference between the AKARI and CGCS positions (Δr = 101″). The AKARI, MSX and 2MASS counterparts based on the IRAS PSC position and CGCS position are different. Therefore, IRAS 16070-4359 and CGCS 3668 seem to be different objects.

IRAS 16103-4929 (CGCS 6624): Epchtein et al. (1990) classified this star as carbon star based on the color index method. Skiff (2014) revealed that the spectral type is M4,M6. Therefore, this star could be a O-rich star with large interstellar extinction.

IRAS 16328-4656 (CGCS 6650): Although Epchtein et al. (1987) first identified this star as a carbon star based on the color index method, it is necessary to confirm the C-rich nature of the central star.

IRAS 17291-3401 (CGCS 3841): Chan & Kwok (1991) first identified it as an SCS based on the CGCS. However, MacConnell (2006) reported it as a M3 star by the NIR spectral observation. This star seems to be misclassified as a carbon star.

IRAS 18252-1011: The C-rich nature is not certain. This star has a large position difference between the AKARI and CGCS positions (Δr = 107″). The AKARI, MSX and 2MASS counterparts based on the IRAS PSC position and CGCS position are different.

IRAS 20476+4422 (CGCS 4993): Although this object has a CGCS counterpart and shows the silicate emission feature at 10 μm, its C-rich nature is not clear.

IRAS 21444+5053: This object is not listed in CGCS and there is no available spectral information to confirm its nature. Jiang et al. (1997) identified this star as a carbon star based on the J-H versus H-K 2CD. However, it was classified as an O-rich star based on the color index method by Guglielmo et al. (1997). Groenewegen et al. (2002) detected CO emission but did not detect HCN and SiO emission. For this object, further investigations are necessary.

4. Subclasses of SCSs

For the 29 confirmed SCSs, we classify them into three subclasses based on the evolutionary stage of the central star. The objects in subclass 1 are five SC/CS

Table 2
The 15 unconfirmed objects which were classified to be SCSs

IRAS PSC	IRAS LRS	CGCS	Spectrum	2CD	Position
06194+1635	E	6139	-	Color based[1]	-
09411−5933	E	6337	M2/3[a]	Color based[2]	-
11311−6355	E	6450	-	Color based[1]	-
12364−6539	F	3263*	M9[a]	-	$\Delta r = 51''$
12569−6105	E	6503	S[b]	Color based[3]	-
13198−6224	E	6526	C[c]; M2[d]	-	-
14286−4706	E	6559	-	Color based[2]	-
16001−4851	E	6612	-	Color based[3]	-
16070−4359	E	3668*	-	Color based[1]	$\Delta r = 101''$
16103−4929	E	6624	M4,M6[a]	Color based[3]	-
16328−4656	E	6650	-	Color based[3]	-
17291−3401	E	3841	M3[e]	-	-
18252−1011	E	4015*	-	-	$\Delta r = 107''$
20476+4422	E	4993	-	-	-
21444+5053	E	-	-	Color based[4]	-

Spectrum: a) Skiff (2014); b) MacConnell (2000); c) Aaronson et al. (1989); d) Lloyd Evans (1991); e) MacConnell (2006); f) Keenan & Boeshaar (1980).
2CD: 1) Guglielmo et al. (1993); 2) Fouque et al. (1992); 3) Epchtein et al. (1990); 4) Jiang et al. (1997).
*The marked object looks to be a different source. See Section 3.

Table 3
The 12 candidate objects which were not verified to be SCSs by Chen & Shan (2011)

IRAS PSC	AKARI PSC	Note	IRAS PSC	AKARI PSC	Note
06462−4157	0647513−420109	candidate	16304−3831	1633527−383752	Probable candidate
15488−4928	1552301−493723	candidate	16469−4753	1650398−475856	Probable candidate
17354−3455	17384548−3457177[a]	candidate	17599−4556	1803383−455637	Probable candidate
17515−2407	1754366−240752	candidate	18038−1614	1806443−161335	Probable candidate
18240−3006	1827159−300439	candidate	18559+0435	1858242+043954	Probable candidate
12195−5527	1222168−554352	Probable candidate	19270+2239	1929101+224542	Probable candidate

[a] The 2MASS counterpart. There is no AKARI counterpart for the object.

stars showing weak silicate emission features. The objects in subclass 2 are 22 carbon stars showing silicate features. In subclass 3, there are two C-rich post-AGB stars showing crystalline silicate features. We list them in Table 4.

The general catalogue of variable stars (GCVS: Samus et al. 2011) contains the list of LPVs for different variable types. LPVs in AGB phase are classified according to the amplitude and regularity of the period into Miras (M), semi-regulars (SR), irregular (L), and RV Tauri type (RV) variables. The GCVS variability type is also listed in Table 4.

In Figure 1, we present the relative spectral energy distributions (SEDs) for the 29 objects. The SEDs show the observational data of USNO-B, 2MASS, WISE, AKARI, IRAS and ISO which cover the wavelength range from 0.9 μm to 100 μm. They show the relative fluxes based on the K band data.

The five objects in subclass 1 are SC/CS stars showing weak silicate emission features. The SC/CS stars (Keenan & Boeshaar 1980) form a continuous spectral sequence intermediate between the S and C stars. They show very strong sodium D-lines, and strong CN bands, and either weak ZrO bands (SC stars) or C$_2$ bands

(CS stars). The molecular abundances indicate a C/O number ratio very close to unity, so that CO formation leaves little C or O for the other molecules. SC or CS stars are likely to be in a transitional phase from an S star to a carbon star. For lower metallicity, stars may go from being O-rich to being carbon stars without any S-type star phase, depending on the dredge-up efficiency and the initial mass of the star (e.g., Iben 1981; Chan and Kwok 1990; Groenewegen et al. 1995). Generally, dust formation in envelopes of S stars is less efficient because of the lack of free O or C to form dust. This could easily explain the weak silicate emission features generally observed in this subclass.

Most stars in subclass 2 show silicate emission features. However, IRAS 03201+5459 shows the silicate absorption feature at 10 μm. And crystalline silicate emission features are observed from IRAS 09425−6040. 11 objects in this subclass are J-type carbon stars (see, e.g., Chen et al. 2007). Groenewegen et al. (1995) argued that the C/O abundance ratio for the star of low initial masses increases in a few and rather larger steps and they probably skip the intermediate state of an S star (C/O∼1) in most cases. The stars in subclass 2 could be in this case. The rich silicate features (see Sec-

Table 4
A new catalog of silicate-carbon stars (29 objects)

IRAS	Other Name	CGCS	LRS	GCVS	Spectrum	Note
1) SC/CS stars with silicate features						
00519+5817	W Cas	136	E	M	SC[1],[14]	C_2H_2+HCN
09083−5158	-	2445	E	-	CS[2]	
18575−0139	VX Aql	4152	E	M:	SC8[1]	
19111+2555	S Lyr	-	E	M	SCe[3]	C_2H_2+HCN
20451+4552	CY Cyg	-	E	LB	SC2[1]	
2) Carbon stars with silicate features (22 objects)						
01373+4000	FBS 0137+400	6019	E	-	C(N)[2]	self-absorption
03201+5459	-	-	U	-	-	C_2H_2+HCN; silicate absorption
06017+1011	-	1158	E	-	C4,5J[4]	H_2O maser
07179+2505	BM Gem	1653	E	SRb	C5,4J[4]	
07204−1032	-	1682	F	-	C4,5J[2]	H_2O maser
08002−3803	Hen 38	2011	E	-	C3,5J[4]	
08577−6035	Mc79 2-11	2406	E	-	C4,5J[4]	H_2O maser
09425−6040	-	-	U	-	-	C_2H_2+HCN; crystalline silicate
11048−6046	-	-	E	-	C:[13]	
10171−6205	-	6359	E	-	C4,4J[2]	
15575−5238	-	6610	E	-	C[12]	
18006−3213	FJF 270	3935	E	-	C5,5J[4]	OH maser
19139+5412	NC 83	4222	E	SR	C[5]	
19451+2856	NSV 12406	4476	E	-	C[8]	
19583−0730	V1468 Aql	4595	E	Lb	C5,5J[4]	
20092+3557	V429 Cyg	4729	E	SRa	C5,4[8]	
20350+5954	V778 Cyg	4923	E	Lb	C4,5J[4]	OH/H_2O maser
21135+5200	12.84	-	E	-	C:[13]	
21566+5309	MQ Cyg	5526	E	M:	C(J)[7]	
22146+6111	-	-	E	-	C[9]	self-absorption
23138+6204	NSV 14477	6912	E	-	C[4]	
23176+4658	EU And	5848	E	Lb:	C4,4J[4]	H_2O maser
3) C-rich post-AGB stars with silicate features						
06176−1036	Red Rectangle	-	P	-	B9-A0[10]	PAH; crystalline silicate
19163+2745	EP Lyr	-	-	RVB	Fp[11]	PAH; crystalline silicate

1) Keenan & Boeshaar (1980); 2) Lloyd Evans (1991); 3) Kwok et al. (1997); 4) Lloyd Evans (1990); 5) Poulakos (1978); 6) Gigoyan & Mickaelian (2012); 7) Chen et al. (2007); 8) Chan (1993); 9) Drew et al. (2005); 10) Cohen et al. (1975); 11) Preston et al. (1963); 12) MacConnell (2003); 13) Kwok et al. (1997); 14) Aoki, Tsuji, & Ohnaka (1998)

tion 4.1) may indicate that the silicate dust formation phase in the previous O-rich atmosphere was relatively recent.

There are two objects in subclass 3. They are C-rich post-AGB stars with crystalline silicate features. These stars show PAH and crystalline silicate features. HD 44179, the central star of the Red Rectangle (IRAS 06176-1036), is known as a spectroscopic binary with a period of 298 days (Van Winckel et al. 1995). EP Lyr (IRAS 19163+2745) is a post-AGB star which is a RV Tau variable with the period of P = 83.46 days (Zsoldos 1995; Gonzalez et al. 1997). RV Tauri stars are luminous evolved stars crossing the instability strip. EP Lyr shows unusually low infrared excess that means a lower dust mass compared to the Red Rectangle.

4.1. The Silicate Features at 10 μm

In order to measure the characteristics of a silicate feature at 10 μm, we assume that the local continuum is a simple power law as follows:

$$\lambda F_{\lambda,cont} = K\lambda^{-p}. \tag{1}$$

where the $\lambda F_{\lambda,cont}$ is the assumed local continuum, K and P are constants to determine. The simple power law was fit to the continuum in the $\sim$8 μm and $\sim$13.5 μm region. The used spectral data for the continuum fitting are IRAS LRS or ISO SWS. After the continuum fitting, we obtain the normalized spectra,

$$S_\lambda = \frac{\lambda F_{\lambda,obs}}{\lambda F_{\lambda,cont}} \tag{2}$$

where $\lambda F_{\lambda,obs}$ is the observed spectrum.

Figure 2 shows the normalized spectra of some SCSs with good quality data. All of the objects are in subclass 2 except S Lyr (subclass 1) and Red Rectangle (subclass 3). They show various shapes of the silicate feature at 10 μm.
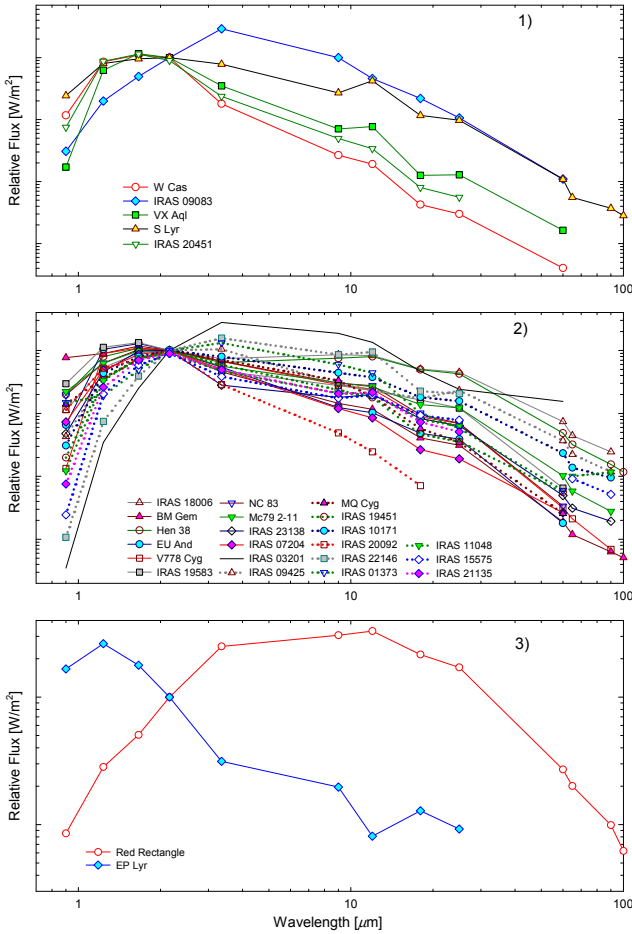
Figure 1. Relative spectral energy distributions for three subclasses. 1) SC/CS stars with silicate emission features; 2) carbon stars with silicate features; 3) C-rich post-AGB stars with crystalline silicate

For S Lyr (subclass 1), the 10 μm feature is very weak. For Red Rectangle (subclass 3), no evident silicate feature at 10 μm is seen but PAH features at 7.7, 8.6 and 11.3 μm as well as crystalline silicate features at longer wavelengths are evident.

For most of the objects in subclass 2, the silicate feature at 10 μm is easily detectable. The dominant feature appears in two objects: V778 Cyg and BM Gem. The 10 μm amorphous silicate feature is less prominent for Hen 38 and IRAS 23138+6204. The feature is weak and flat for IRAS 09425-6040, IRAS 10170-6205. The 10 μm absorption feature of amorphous silicate is identified for IRAS 03201+5459.

The 11.3 μm emission feature seen in spectra of IRAS 03201+5459 and 09425-6040 (subclass 2) can be caused by SiC, PAH or crystalline forsterite. However, 11.3 μm emission features due to PAH or crystalline forsterite are narrower and involve other features at other wavelengths. There is no other conspicuous features indicating PAH or crystalline silicate in the spectra of IRAS 03201+5459 and 09425-6040. Therefore, the emission feature at 11.3 μm is likely to be caused by SiC grains.
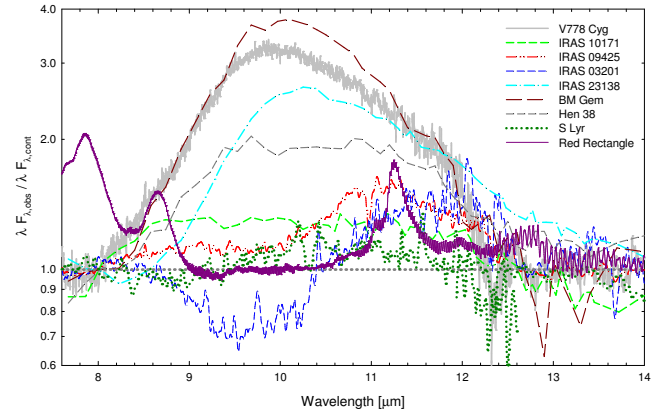
Figure 2. Profile lines of the observed 10μm silicate feature.

For some of the SCSs in subclass 2 (e.g., IRAS 10171-6205 and Hen 38), the silicate feature at 10 μm is weak and flat. Kessler-Silacci et al. (2006) argued the weak and flat features of amorphous silicate can be interpreted as grain growth (from 0.1 to 1.0 μm in radius). The unusual silicate features in the SCSs indicate that the dust grains experience significant chemical and physical processing in their environment. Generally, a suitable site for grain growth is believed to be a stationary disk rather than an expanding shell. The weak and flat silicate feature may imply dust processing in a long lived reservoir such as a disk.

5. Dust Shell Models for the Chemical Transition Phase

To investigate the effect of the chemical transition phase from O to C, we use simple radiative transfer models for the detached silicate dust shells. The spectral energy distributions and infrared color-color diagrams of SCSs are compared with the theoretical model results.

5.1. Radiative Transfer Model Calculations

In this work, we use the radiative transfer code RADMC-3D (http://www.ita.uni-heidelberg.de/~dullemond/software/radmc-3d/) to calculate the model SEDs. RADMC-3D is the three-dimensional version of the code for investigating dust continuum radiative transfer processes based on the Monte Carlo simulation method of Bjorkman & Wood (2001). For this work, we consider the geometry of one-dimensional grid only. Given spherically symmetric density structures, the code calculates the dust temperature and scattering source function at every geometric point in the model. Model SEDs can be calculated by integrating the intensity inside synthetic observing apertures at each wavelength.

5.2. Basic Model Parameters

In this paper, we assume a spherically symmetric dust shell around a single star. We use similar schemes for dust density distribution as those used by Suh & Kwon

(2013). Although AGB stars are pulsating, the overall continuous density distribution is believed to be maintained for a time scale larger than the pulsation period (e.g., Suh 1999; Suh 2004).

In this paper, we assume that the dust density distribution is continuous ($\rho \propto r^{-2}$) from the inner radius (R_{in}) to the outer radius (R_{out}) for each dust shell. For the dust density distribution of a spherically symmetric dust shell, we use the simple power law equation

$$\rho(r) = \beta \rho_{in}(r/R_{in})^{-2}, \qquad (3)$$

where ρ_{in} is the density at R_{in} of the dust shell.

The inner shell dust temperature (T_c) is the dust temperature at R_{in}. In model calculations, we may find R_{in} at which the dust temperature (T_c) becomes the desired one after a few trials. The model SEDs are sensitively dependent on T_c. We may roughly regard the temperature T_c as the dust formation (or condensation) temperature. However, T_c is not necessarily the same as the dust formation temperature, depending on the physical conditions of pulsating OH/IR stars (see Suh 2004).

For the central star, we assume that the luminosity is 1×10^4 $L_\odot$ and a stellar blackbody temperature is 2500 K.

5.3. The Model Setup

We investigate the time scales for the appearance of the silicate feature after the chemical transition of the central star from O to C which is characterized by a sudden cessation of the O-rich mass-loss. Because the central star does not provide O-rich material after the chemical transition, the silicate dust shell will be detached gradually from the central star and the silicate dust features will become weaker. The transition object with a C-rich central star can be classified to be a SCS until the silicate dust feature completely disappears. Previously estimated time scale for the transitional object as a SCS is predicted to last only a few decades (e.g., Little-Marenin et al. 1988).

The initial inner radius (R_0) of dust shell is chosen by the radius where the dust temperature is 1000 K. As the dust shell expands, the inner radius (R_{in}) of the dust shell increases with time ($R_{in} = R_0 + V_{exp}t$) after the chemical transition begins (or the O-rich mass-loss stops at R_0).

We use spherically symmetric O-rich dust shells with four different dust optical depths of $\tau_{10,int} = 0.01$, 0.1, 1 and 7 as the initial conditions. For all of the models, we assume that the stellar wind velocity V_{exp} is constant. We use the dust opacity functions of warm ($\tau_{10,int} = 0.01$, 0.1 and 1) and cold ($\tau_{10,int} = 7$) amorphous silicate derived by Suh (1999). We assume that all dust grains are spherical with a uniform radius of 0.1 μm and the scattering is assumed to be isotropic.

For each model, the dust temperature (T_c) at the R_{in} decreases as the O-rich dust shell expands. We fixed the outer radius (R_{out}) of the dust shell to 10^5 AU (~ 0.5 pc). For the all of the models, dust temperatures at

R_{out} are lower than 30 K which is comparable to the temperature of interstellar medium.

5.4. Evolution of the Silicate Feature

In Figure 3, we present the profile lines of the silicate feature at 10 μm obtained from the model SEDs of the transitional dust shells explained in Section 5.3. As explained in Section 3.1, the normalized model spectra are obtained using the local continuum Equation (1). As the dust shell expands, the strength of the silicate emission feature becomes weak and the peak of the feature moves slightly to longer wavelengths. We may claim that the silicate feature disappears when the following condition is satisfied around 10 μm:

$$\frac{F_{cal,\lambda}}{F_{cont,\lambda}} - 1 < 0.05, \qquad (4)$$

where $F_{cal,\lambda}$ is the calculated flux. We find that the silicate emission feature for the expanding O-rich shell is retained only for a short time and fade away rapidly. We assume that the shell expands outward with a constant velocity of 10 km/sec (e.g., Loup et al. 1993) thereby moving 210 AU in 100 years. The life time scales for the silicate emission feature for the models of $\tau_{10,int} = 0.01$, 0.1, 1 and 7 are about 50, 140, 380 and 400 years, respectively.

As the O-rich dust shell expands, silicate emission features disappear due to fast dilution of silicate dust density and/or cooling of dust temperature (< 150 K) (See Table 4) . For the model of $\tau_{10,int} = 7$, the silicate absorption feature at 10 μm is retained only for a short time scale (~ 28 years). Then the silicate emission feature lasts for about 380 years.

Though the transition models reproduce various shapes of the silicate feature, they can not reproduce the flat silicate features seen in some of the SCSs (e.g., IRAS 10171-6205). Other theoretical models (e.g., a disk model) could be more useful.

6. Two-Color Diagrams

We present the IRAS 2CDs for AGB stars using [25]-[60] versus [12]-[25] in Figure 4 and the NIR-IRAS 2CD using [12]-[25] versus K-L in Figure 5. See Suh & Kwon (2011) for detailed explanations about the color indices. We use available NIR data in K and L bands obtained from ground-based observations as explained in Suh & Kwon 2011. We plot the observed colors of 29 SCSs verified in this paper and 15 unconfirmed objects and 12 candidate objects presented by CS11. We also plot the observed colors of 3373 O-rich AGB stars listed in Kwon & Suh (2012) and 1168 C-rich AGB stars for comparison.

For any 2CD, we use only objects with a good photometric quality flag (q = 3) to plot at any wavelength. We also plot the results of model calculations for the spherical dust shell models presented in Section 5 for comparison.

Each model track on the 2CD is composed of 24 points of different inner radii of dust shell from r_1 to
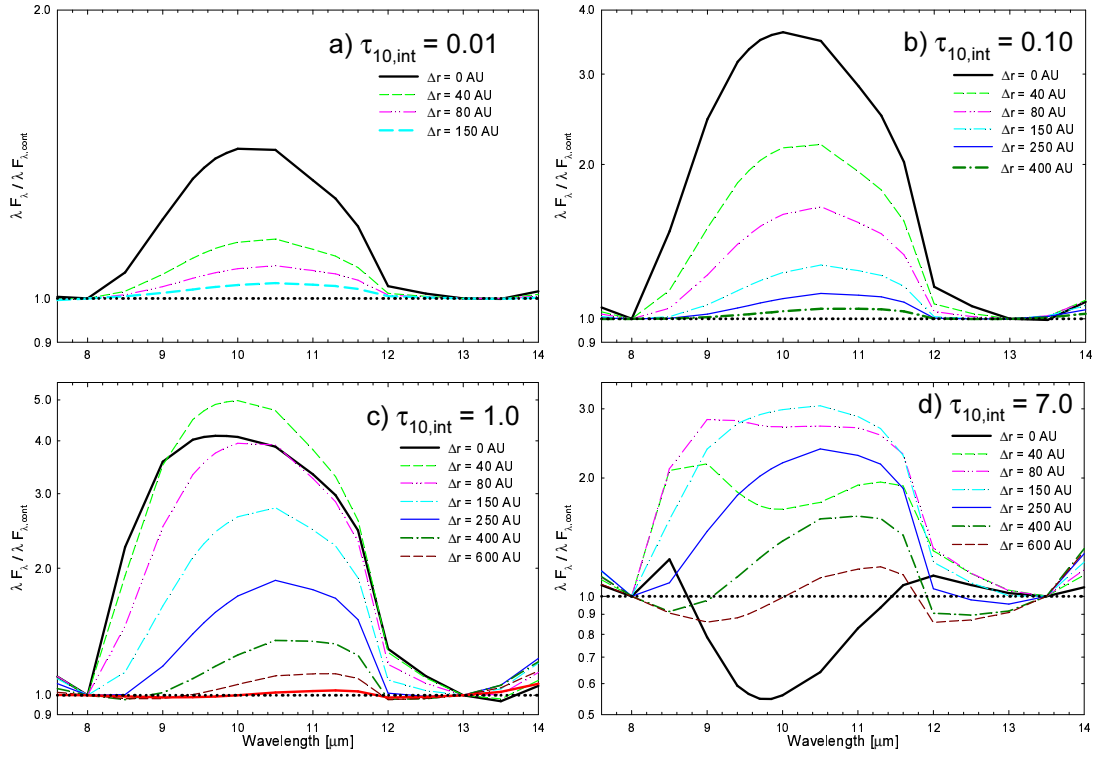
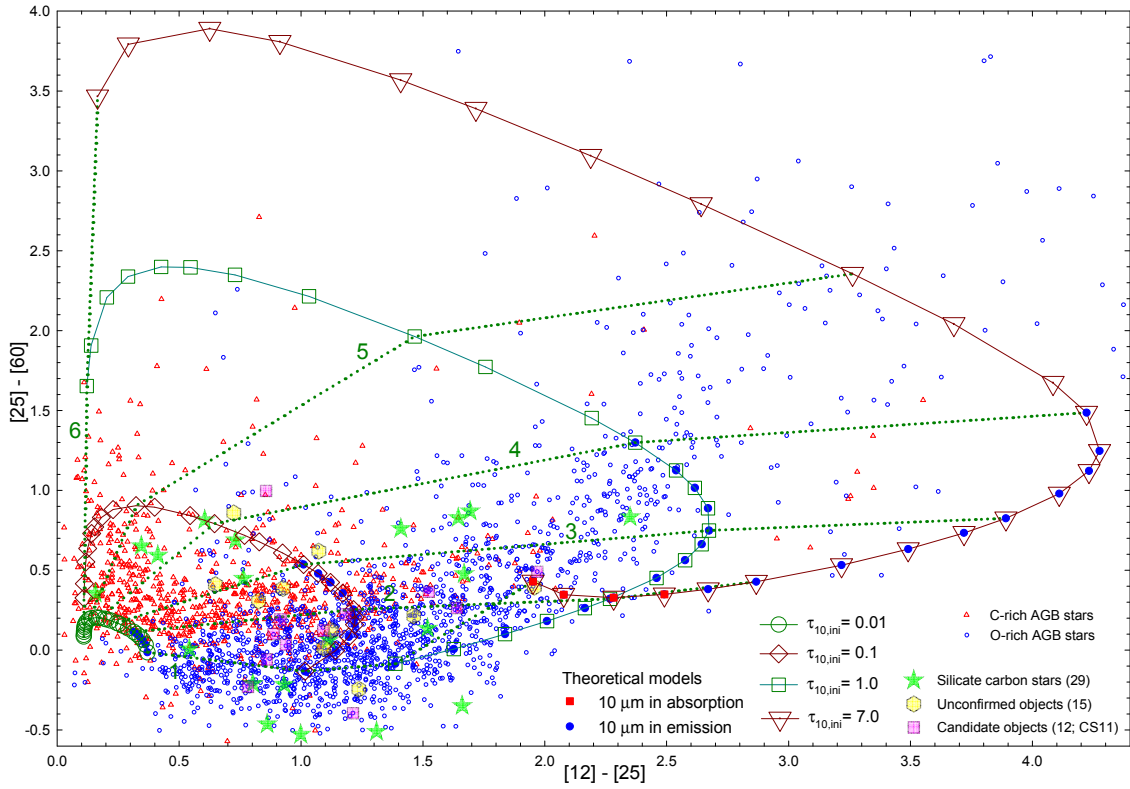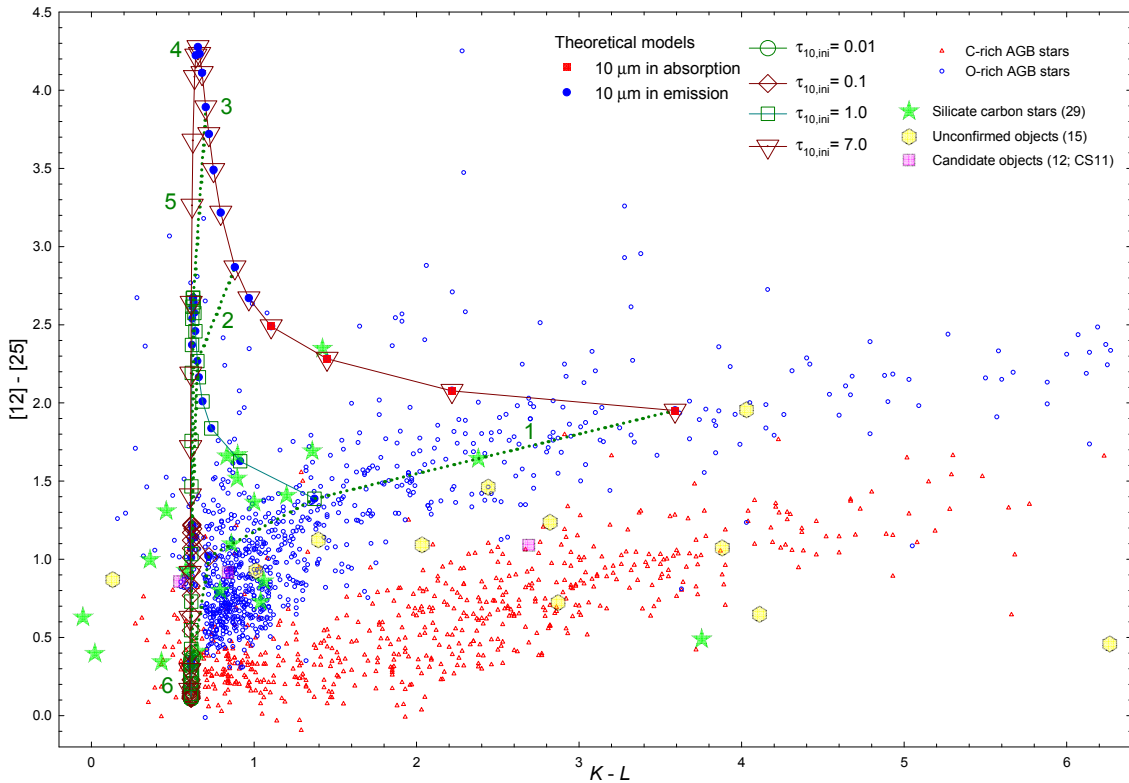**Figure 3.** Profile lines of the silicate 10μm feature for the transitional models.

Figure 4. The IRAS 2CD ([25]-[60] versus [12]-[25]).

Figure 5. The NIR-IRAS 2CD ([12]-[25] versus K-L).

r_1+15000 AU. The amount of shell detachment ($\Delta r = V_{exp}t$) corresponds to the time steps from 0 to about 10000 years under the condition of $V_{exp} = 10$ km/s. We examine the shape of the silicate feature at 10 μm to determine the silicate emission or absorption phases as explained in Section 5.4. We represent the silicate absorption phases by red filed squares and the emission phases by blue filled cicles on the 2CDs.

In Table 5, we list the model parameters of $\tau_{10} = 0.01, 0.1, 1$ and 7 for six time step points which are also labeled in the 2CDs. The inner radius(R_{in}) of the dust shell, dust density (ρ_{in}) at the inner radius, dust temperature (T_c) at the inner radius and τ_{10} of each model are listed. The points labeled with number 1 indicate the initial points for normal O-rich AGB stars. The points labeled as 2, 3 and 4 refer to the end point of silicate emission phase for the model of $\tau_{10} = 0.01, 0.1$ and 1, respectively. The points 5 and 6 are the model points for the expansion times of $\sim$1000 and $\sim10^4$ years, respectively.

The loop-like shape of evolutionary tracks on the [25]-[60] versus [12]-[25] diagram (Figure 4) resemble the works of Willems & de Jong (1988) and Chan & Kwok (1988). The model tracks show that the silicate emission feature remains toward higher values of [12]-[25] color but disappears for higher values of [25]-[60] color. Although some SCSs are located around the model track on the [25]-[60] versus [12]-[25] diagram, the model can not cover the wide distributions of ob-

served SCSs. Although it takes less time to show silicate features in the transition model, the expanding shell can contribute to far-IR continuum emission for a much longer time scale. As we can see in Figure 4, the flux excesses at 60 μm relative to O-rich AGB stars are due to the cooling dust remnants ejected at least $\sim$100 and 1000 years ago for the models of $\tau_{10} = 0.01$ and 7, respectively. These model tracks for later stages are particularly successful in explaining the SCSs in the upper-left region of the 2CD where optical carbon stars are located.

In the [12]-[25] versus K-L diagram (Figure 5), the model tracks develop toward the upper left region to converge quickly (less than 500 years) to the vertical line of K-$L \simeq 0.6$. Many of the SCSs are outside the regions of the transition model tracks. This is because carbon stars show strong photospheric molecular bands in K and L which can skew the K-L color value away from what is expected for a blackbody of 2500 K. Note that the time scale for the model tracks is relatively short ($\sim$1000 years from the label point 1 to point 5).

Contrary to previous works (Willems & de Jong 1988; Chan & Kwok 1988), our results show that the life time of the silicate feature can be much longer (up to 400 years depending on the initial dust optical depth; see Section 5.4). This is because we use higher initial dust optical depths ($\tau_{10} = 1$ and 7) which are appropriate for some observed SCSs (e.g., the IRAS 03201+5459 shows the 10 μm silicate feature in absorption) as well

Table 5
Parameters for the transitional dust shell models

$\tau_{10,int}$	Parameters	1	2 (47 years)	3 (142 years)	4 (400 years)	5 ($\sim 10^3$ years)	6 ($\sim 10^4$ years)
0.01	R_{in} [AU]	12.9	116.4	312.6	839	2059	20321
	ρ_{in} [g/cm^3]	2.75E-20	3.38E-22	4.69E-23	6.51E-24	1.08E-24	1.11E-26
	T_c [K]	1001	324	207	140	100	46
	τ_{10}	0.01	1.1E-3	4.1E-4	1.5E-4	6.1E-5	5.0E-6
	Silicate*	Emission	Emission	No	No	No	No
0.1	R_{in} [AU]	13.4	113.8	322.8	829	2027	20461
	ρ_{in} [g/cm^3]	2.64E-19	3.69E-21	4.58E-22	6.94E-23	1.16E-23	1.14E-25
	T_c [K]	1001	329	205	141	101	46
	τ_{10}	0.1	0.012	4.2E-3	1.6E-3	6.5E-4	5.2E-5
	Silicate*	Emission	Emission	Emission	No	No	No
1.0	R_{in} [AU]	15.7	118.6	325.5	818	2056	20150
	ρ_{in} [g/cm^3]	2.25E-18	3.97E-20	5.28E-21	8.35E-22	1.32E-22	2.33E-24
	T_c [K]	999	331	206	142	100	46
	τ_{10}	1.0	0.13	0.048	0.019	7.5E-3	6.2E-4
	Silicate*	Emission	Emission	Emission	Emission	No	No
7.0	R_{in} [AU]	18.3	122.1	329.2	851	2105	21621
	ρ_{in} [g/cm^3]	1.22E-17	2.74E-19	3.77E-20	5.64E-21	9.22E-22	8.73E-24
	T_c [K]	1000	336	167	130	93	43
	τ_{10}	7.0	1.05	0.351	0.136	0.0549	5.34E-3
	Silicate*	Absorption	Emission	Emission	Emission	No	No

*The silicate feature at 10 μm.

as smaller ones ($\tau_{10} = 0.01$ and 0.1). The previous works considered only the SCSs with the initial 10 μm silicate feature in emission ($\tau_{10} < 1$).

7. Discussion

As explained in Sections 5.4 and 6, we find that the detached silicate dust shell models can not explain the observed SEDs for the whole sample of SCSs. We may need a more complicated geometry for the dust distribution. A more sophisticated theoretical model using a circumbinary or circumstellar dust disk as well as the dust shell would be more useful.

There are some observational evidences for the presence of a disk in some SCSs. For BM Gem and EU And, the variations of radial velocity are detected due to motions in a binary system by Barnbaum et al. (1991). And Kahane et al. (1998) and Jura & Kahane (1999) observed the narrow CO emission lines supporting the presence of long-lived reservoirs of orbiting gas in the two stars. Izumiura et al. (2008) found the P Cygni-type profile in the violet spectra of BM Gem which indicates the presence of an outflow with at least 400 km/s. Ohnaka et al. (2008) made mid-IR interferometry observations toward BM Gem which suggested a circum-companion disk. And VLBA H$_2$O maser observations toward EU And supported the circum-companion disk (Ohnaka & Boboltz 2008). For V778 Cyg, Szczerba et al. (2006) obtained high resolution H$_2$O maser maps at 22 GHz and they concluded that the object is composed of a C-rich star and a companion that stores an O-rich disk. Those observations are strong evidences for presence of an O-rich disk around a SCS which is actually a binary system. We expect that most SCS are likely to be binary systems rather than single stars.

8. Summary

We have collected 44 SCSs from the literature and verified their classification. We have confirmed that 29 objects are real SCSs and 15 objects are unconfirmed. For some objects, it is doubtful whether the central star is a carbon star. Other objects seem to be contaminated by interstellar clouds.

For the confirmed 29 SCSs, we have classified them into three subclasses based on the evolution phase of the central star: SC/CS stars with silicate emission features, carbon stars with silicate features and C-rich post-AGB stars with crystalline silicate. The shapes of the silicate emission feature at 10 μm for various SCSs have been investigated.

We have made radiative transfer model calculations for the transitional dust shell models of SCSs with detached O-rich dust shells. We have compared the theoretical model results with the observations of SCSs on different 2CDs. The life time of the silicate emission feature at 10 μm has been estimated to be 50-400 years depending on the thickness of the dust shell in the O-rich phase. For model of $\tau_{10,ini} = 7$, silicate absorption phase appears only for a short time scale.

The transitional dust shell models presented in this paper may provide only a partial explanation for the origin of SCSs because the models do not reproduce all of the observations. For the chemical transition model without considering the effect of a disk, the life time of the silicate feature is too short. We expect that a more sophisticated theoretical model using a circumbinary or circumstellar dust disk as well as the dust shell would be useful.

REFERENCES

Aaronson, M., Blanco, V. M., Cook, K. H., et al. 1989, Southern Milky Way Carbon Stars - New Candidates, JHK Photometry, and Radial Velocities, ApJS, 70, 637

Alksnis, A., Balklavs, A., Dzervitis, U., et al. 2001, General Catalog of galactic Carbon stars, 3d Ed., Balt. Astron., 10, 1

Aoki, W., Tsuji, T., & Ohnaka, K. 1998, Infrared Spectra of Carbon Stars Observed by the ISO SWS I. Molecular Absorption in N-Type and SC-Type Stars, A&A, 340, 222

Barnbaum, C., Kastner, J. H., Morris, M., et al. 1991, Carbon Stars Associated with Oxygen-Rich Circumstellar Envelopes - EU Andromedae, BM Geminorum and V 778 Cygni, A&A, 251, 79

Bjorkman, J. E., & Wood, K. 2001, Radiative Equilibrium and Temperature Correction in Monte Carlo Radiation Transfer, ApJ, 554, 615

Busso, M., Gallino, R., & Wasserburg, G. J. 1999, Nucleosynthesis in Asymptotic Giant Branch Stars: Relevance for Galactic Enrichment and Solar System Formation, ARAA, 37, 239

Chan, S. J. 1993, Spectroscopic Study of Carbon Stars with Silicate Features. 1: Observations, AJ, 106, 2126

Chan, S. J., & Kwok, S. 1988, The Transition from Oxygen-Rich to Carbon Stars, ApJ, 334, 362

Chan, S. J., & Kwok, S. 1990, Evolution of Infrared Carbon Stars, A&A, 237, 354

Chan, S. J., & Kwok, S. 1991, New Candidates for Carbon Stars with Silicate Features, ApJ, 383, 837

Chen, P.-S., & Yang, X.-H., Zhang, P. 2007, Infrared Study of J-Type Carbon Stars Based on Infrared Astronomical Satellite, Two Micron All Sky Survey, and Infrared Space Observatory Data, AJ, 134, 214

Chen, P.-S., & Shan, H.-G. 2011, Identification of New Silicate Carbon Stars, ApSS, 335, 457

Cohen, M., Anderson, C. M., Cowley, A., et al. 1975, The Peculiar Object HD 44179 'The Red Rectangle', ApJ, 196, 179

Cutri, R. M., Skrutskie, M. F., Van Dyk, S., et al. 2003, The IRSA 2MASS All-Sky Catalog of Point Sources. In: NASA/IPAC Infrared Science Archive

Drew, J. E., Greimel, R., & Irwin, M. J. 2005, The INT Photometric H Survey of the Northern Galactic Plane (IPHAS), MNRAS, 362, 753

Egan, M. P., Price, S. D., & Kraemer, K. E. 2003, The Midcourse Space Experiment Point Source Catalog Version 2.3, BAAS, 203, 5708

Engels, D. 1994, More H2O Maser in J-Type Carbon Stars, A&A, 285, 497

Epchtein, N., Le Bertre, T., Lepine, J. R. D., et al. 1987, Valinhos 2.2 Micron Survey of the Southern Galactic Plane. II - Near-IR Photometry, IRAS Identifications and Nature of the Sources, A&AS, 71, 39

Epchtein, N., Le Bertre, T., & Lepine, J. R. D. 1990, Carbon Star Envelopes - Near-IR Photometry, Mass Loss and Evolutionary Status of a Sample of IRAS Stars, A&A, 227, 82

Fouque, P., Le Bertre, T., & Epchtein, N. 1992, Near-Infrared Photometry of a Sample of IRAS Point Sources, A&AS, 93, 151

Gielen, C., Van Winckel, H., Min, M., et al. 2008, SPITZER Survey of Dust Grain Processing in Stable Discs around Binary Post-AGB Stars, A&A, 490, 725

Gielen, C., Van Winckel, H., Matsuura, M., et al. 2009, Analysis of the Infrared Spectra of the Peculiar Post-AGB Stars EP Lyrae and HD 52961, A&AS, 503, 843

Gigoyan, K. S., & Mickaelian, A. M. 2012, Revised and Updated Catalogue of the First Byurakan Survey of Late-Type Stars, MNRAS, 419, 3346

Gonzalez, G., Lambert, D. L., & Giridhar, S. 1997, Abundance Analyses of the Field RV Tauri Variables: EP Lyrae, DY Orionis, AR Puppis, and R Sagittae, ApJ, 479, 427

Groenewegen, M. A. T., van den Hoek, L. B., & de Jong, T. 1995, The Evolution of Galactic Carbon Stars., A&A, 293, 381

Groenewegen, M. A. T., Sevenster, M., Spoon, H. W. W., et al. 2002, Millimetre Observations of Infrared Carbon Stars. I. The data, A&A, 390, 501

Guglielmo, F., Epchtein, N., Le Bertre, T., et al. 1993, Identification of 106 New Infrared Carbon Stars in the IRAS Point Source Catalog - Near-Infrared Photometry and Their Space Distribution in the Galaxy, A&AS, 99, 31

Guglielmo, F., Epchtein, N., Arditti, F., et al. 1997, New Infrared Carbon Stars in the IRAS Point Source Catalog., A&AS, 122, 489

Iben, Jr. I. 1981, The Carbon Star Mystery - Why Do the Low Mass Ones Become Such, and Where Have All the High Mass Ones Gone, ApJ, 246, 278

Izumiura, H., Noguchi, K., Aoki, W., et al. 2008, Evidence for a Companion to BM Gem, a Silicate Carbon Star, ApJ, 682, 499

Jiang, B. W., Deguchi, S., Hu, J. Y., et al. 1997, Identification of IRAS Sources in the Outer Disk of the Galaxy, AJ, 113, 1315

Jura, M., & Kahane, C. 1999, Orbiting Molecular Reservoirs around Evolved Red Giant Stars, ApJ, 521, 302

Kahane, C., Barnbaum, C., Uchida, K., et al. 1998, A Circumbinary Reservoir around BM Geminorum?, ApJ, 500, 466

Keenan, P. C., & Boeshaar, P. C. 1980, Spectral Types of S and SC Stars on the Revised MK System, ApJS, 43, 379

Kessler-Silacci, J., Augereau, J., Dullemond, C. P., et al. 2006, c2d Spitzer IRS Spectra of Disks around T Tauri Stars. I. Silicate Emission and Grain Growth, A&A, 639, 275

Kwok, S., Volk, K., & Bidelman, W. P. 1997, Classification and Identification of IRAS Sources with Low-Resolution Spectra, ApJS, 112, 557

Kwon, Y.-J., & Suh, K.-W. 2012, Properties of OH, SiO, and H2O Maser Emission in O-Rich AGB Stars, JKAS, 45, 139

Little-Marenin, I. R. 1986, Carbon Stars with Silicate Dust in Their Circumstellar Shells, ApJL, 307, L15

Little-Marenin, I. R., Benson, P. J., & Dickinson, D. F. 1988, Masers Associated with Two Carbon Stars - V778 Cygni and EU Andromedae, ApJ, 330, 828

Lloyd Evans, T. 1990, Carbon Stars with Silicate Dust Shells. I - Carbon Stars with Enhanced C-13 (J Stars),

MNRAS, 243, 336

Lloyd Evans, T. 1991, Carbon Stars with Silicate Dust Shells. II - More Stars with Enhanced C-13 (J Stars), MNRAS, 249, 409

Loup, C., Forveille, T., Omont, A., & Paul, J. F. 1993, CO and HCN Observations of Circumstellar Envelopes. A Catalogue - Mass Loss Rates and Distributions, A&AS, 99, 291

MacConnell, D. J. 2000, New S Stars Found in a Southern Galactic Plane Survey, PASP, 112, 65

MacConnell, D. J. 2003, Southern Cool Carbon Stars Found on Near-Infrared Objective Prism Plates, PASP, 115, 351

MacConnell, D. J. 2006, Southern Cool Stars Misclassified as Carbon Stars, Inf. Bull. Var. Stars, 5671, 1

Molster, F. J., Yamamura, I., Waters, L. B. F. M., et al. 2001, IRAS 09425-6040: A Carbon Star Surrounded by Highly Crystalline Silicate Dust, A&A, 366, 923

Monet, D. G., Levine, S. E., Canzian, B., et al. 2003, The USNO-B Catalog, AJ, 125, 984

Morris, M. 1987, Mechanisms for Mass Loss from Cool Stars, PASP, 99, 1115

Murakami, H., Baba, H., Barthel, P., et al. 2007, The Infrared Astronomical Mission AKARI, PASJ, 59, 369

Ohnaka, K., & Boboltz, D. A. 2008, Imaging the Oxygen-Rich Disk toward the Silicate Carbon Star EU Andromedae, A&A, 478, 809

Ohnaka, K., Izumiura, H., Leinert, C., et al. 2008, Asymmetric Silicate Dust Distribution toward the Silicate Carbon Star BM Geminorum, A&A, 490, 173

Poulakos, C. 1978, Extremely Red Stars at $e^{II} \approx 113°$, $-10° \leq b^{II} \leq 90°$, A&AS, 32, 395

Preston, G. W., Krzeminski, W., Smak, J., et al. 1963, A Spectroscopic and Photoelectric Survey of the RV Tauri Stars, ApJ, 137, 401

Samus, N. N., Durlevich, O. V., Kazarovets, E. V., Kireeva, N. N., Pastukhova, E. N., & Zharova, A. V. 2011, General Catalog of Variable Stars (GCVS database, Version 2011Jan), VizieR online data catalogue, B/GCVS

Skiff, B. A. 2014, General Catalogue of Stellar Spectral Classifications (Version 2013-Jul), VizieR B/mk

Suh, K.-W. 1999, Optical Properties of the Silicate Dust Grains in the Envelopes around Asymptotic Giant Branch Stars, MNRAS, 304, 389

Suh, K.-W. 2000, Optical Properties of the Carbon Dust Grains in the Envelopes around Asymptotic Giant Branch Stars, MNRAS, 315, 740

Suh, K.-W. 2004, Pulsation Phase-Dependent Dust Shell Models for Oxygen-rich Asymptotic Giant Branch Stars, ApJ, 615, 485

Suh, K.-W., & Kwon, Y.-J. 2011, Infrared Two-Colour Diagrams for AGB Stars Using AKARI, MSX, IRAS and Near-Infrared Data, MNRAS, 417, 3047

Suh, K.-W., & Kwon, Y.-J. 2013, Water Ice in High Mass-Loss Rate OH/IR Stars, ApJ, 762, 113

Szczerba, R., Szymczak, M., Babkovskaia, N., et al. 2006, Oxygen-Rich Disk in the V778 Cygni System Resolved, A&A, 452, 561

te Lintel Hekkert, P. 1991, An OH Survey of Very Cold IRAS Point Sources, A&A, 248, 209

Van Winckel, H., Waelkens, C., & Waters, L. B. F. M. 1995, The Extremely Iron-Deficient "Post-AGB" Stars and Binaries., A&A, 293, 25

Willems, F. J., & de Jong, T. 1986, Carbon Stars with Oxygen-Rich Circumstellar Dust Shells Observational Evidence for the Onset of the Carbon Star Phase, ApJL, 309, 39

Willems, F. J., & de Jong, T. 1988, IRAS Low Resolution Spectra of Cool Carbon Stars. IV - A Scenario for Carbon Star Evolution, A&A, 196, 173

Wright, E. L., Eisenhardt, P. R. M., Mainzer, A. K., et al. 2010, The Wide-Field Infrared Survey Explorer (WISE): Mission Description and Initial On-Orbit Performance, AJ, 140, 1868

Yamamura, I., Dominik, C., de Jong, T., et al. 2000, The Origin of Silicate Carbon Stars: ISO/SWS Observation of V778 Cygni, A&A, 363, 629

Zsoldos, E. 1995, Photometry of EP Lyrae and Period Changes in RV Tauri Stars, A&A, 296, 122